

Gurimite, $\text{Ba}_3(\text{VO}_4)_2$ and hexacelsian, $\text{BaAl}_2\text{Si}_2\text{O}_8$ – two new minerals from schorlomite-rich paralava of the Hatrurim Complex, Negev Desert, Israel

IRINA O. GALUSKINA^{1,*}, EVGENY V. GALUSKIN¹, YEVGENY VAPNIK², KRYSYAN PRUSIK³, MARTA STASIAK¹, PIOTR DZIERŻANOWSKI⁴ AND MIKHAIL MURASHKO⁵

¹ Faculty of Earth Sciences, Department of Geochemistry, Mineralogy and Petrography, University of Silesia, Będzińska 60, 41-200 Sosnowiec, Poland

² Department of Geological and Environmental Sciences, Ben-Gurion University of the Negev, POB 653, Beer-Sheva 84105, Israel

³ Institute of Materials Science, University of Silesia, 75 Pułku Piechoty 1A, 41-500 Chorzów, Poland

⁴ Institute of Geochemistry, Mineralogy and Petrology, University of Warsaw, al. Żwirki i Wigury 93, 02-089 Warszawa, Poland

⁵ Saint Petersburg State University, Faculty of Geology, 7-9 Universitetskaya nab., St Petersburg, 199034, Russia

[Received 21 June 2016; Accepted 9 September 2016; Associate Editor: Sergey Krivovichev]

ABSTRACT

Two new barium-bearing minerals: gurimite, $\text{Ba}_3(\text{VO}_4)_2$ (IMA2013-032) and hexacelsian, $\text{BaAl}_2\text{Si}_2\text{O}_8$ (IMA2015-045) were discovered in veins of paralava cutting gehlenite-flamite hornfels located in the Gurim Anticline in the Negev Desert, Israel. Gurimite and hexacelsian occur in oval polymineralic inclusions in paralava and are associated with gehlenite, pseudowollastonite or wollastonite, rankinite, flamite, larnite, schorlomite, andradite, fluorapatite, fluorellestadite, kalsilite, cuspidine, aradite, zadovite and khesinite. Gurimite and hexacelsian form elongate crystals $<10 \mu\text{m}$ thick. The minerals are colourless and transparent with a white streak and vitreous lustre, and have (0001) cleavage, respectively good in gurimite and very good in hexacelsian. Fracture is irregular. Density calculated using empirical formulas gave 5.044 g cm^{-3} for gurimite and 3.305 g cm^{-3} for hexacelsian. Mean refractive indexes, 1.945 and 1.561, respectively, were also calculated using the empirical formulas and the Gladstone-Dale relationship. The minerals are uniaxial and nonpleochroic. The following empirical crystal chemical formulae were assigned to holotype gurimite: $(\text{Ba}_{2.794}\text{K}_{0.092}\text{Ca}_{0.084}\text{Na}_{0.033}\text{Sr}_{0.017})_{\Sigma 3.020}(\text{V}_{1.827}^{5+}\text{S}_{0.091}^{6+}\text{P}_{0.051}^{5+}\text{Al}_{0.040}\text{Si}_{0.005}\text{Fe}_{0.005}^{3+})_{\Sigma 2.017}\text{O}_8$, and holotype hexacelsian: $(\text{Ba}_{0.911}\text{K}_{0.059}\text{Ca}_{0.042}\text{Na}_{0.010})_{\Sigma 1.022}\text{Al}_{1.891}\text{Fe}_{0.072}^{3+}\text{Si}_{2.034}\text{O}_8$. The Raman spectrum of hexacelsian is similar to the one of the synthetic disordered β - $\text{BaAl}_2\text{Si}_2\text{O}_8$. The Raman spectrum of gurimite is identical to that of synthetic $\text{Ba}_3(\text{VO}_4)_2$. The electron back-scattered diffraction (EBSD) pattern of gurimite was fitted to the structure of its synthetic analogue with the cell parameters of $R\bar{3}m$, $a = 5.784(1)$, $c = 21.132(1)$ Å, $V = 612.2(2)$ Å³, $Z = 3$, giving a mean angular deviation = 0.43° (good fit). The Raman spectra of hexacelsian and its EBSD pattern suggest that natural hexacelsian corresponds to disordered synthetic β -hexacelsian $P6_3/mcm$, $a = 5.2920(4)$ Å, $c = 15.557(2)$ Å, $\alpha = \beta = 90^\circ$, $\gamma = 120^\circ$. We suggest that after relatively fast crystallization of the main constituents of the paralava, gurimite, hexacelsian and also other Ba-bearing phases crystallized from residual melt enriched in incompatible elements that filled interstices between crystals of the main constituents.

KEYWORDS: gurimite, hexacelsian, electron back-scattered diffraction method, Raman, schorlomite-rich paralava, Negev Desert, Israel.

Introduction

*E-mail: irina.galuskina@us.edu.pl
<https://doi.org/10.1180/minmag.2016.080.147>

NEW Ba-bearing minerals gurimite, $\text{Ba}_3(\text{VO}_4)_2$ (IMA2013-032), $R\bar{3}m$, $a = 5.784(1)$ Å, $c =$

21.132(1) Å, $V=612.2(2)$ Å³), and hexacelsian, BaAl₂Si₂O₈ (IMA2015-045, $P6_3/mcm$, $a=5.292(1)$, $c=15.557(2)$ Å), were found in thin veins considered to be paralava by Sharygin *et al.* (2006a,b). The paralavas are widespread within gehlenite-flamite hornfels of the Hatrurim Complex (the 'Mottled Zone'; Bentor, 1960; Gross, 1977; Vapnik *et al.*, 2007) in Gurim Anticline, Hatrurim Basin (N 31°12' E 35°14'), located near the town of Arad in the Negev Desert, Israel. The paralava is a coarse-grained rankinite-pseudowollastonite-schorlomite-gehlenite rock resembling a pegmatite rather than an effusive rock. Recently, two new Ba-bearing minerals with an antiperovskite structure belonging to the isomorphic series of zadovite, BaCa₆[(SiO₄)(PO₄)](PO₄)₂ – aradite, BaCa₆[(SiO₄)(VO₄)](VO₄)₂ (Galuskin *et al.*, 2015), as well as the Fe³⁺-analogue of synthetic phase SFCAM, khesinite, Ca₄(Mg₂Fe₁₀³⁺)O₄[(Fe₁₀³⁺Si₂)O_{3c}] (Galuskina *et al.*, 2017), were described in the paralava.

Gurimite and hexacelsian have synthetic analogues. Synthetic barium orthovanadate, Ba₃(VO₄)₂ is a potential matrix for phosphorus, it exhibits intense rare-earth activated luminescence and can be used in television tubes, luminescent lamp coatings and solid-state lasers (Susse and Buerger, 1970; Azdouz *et al.*, 2010). Until recently the only known Ba minerals in the feldspar group were celsian and paracelsian (Black, 2014). Synthetic polymorphs of celsian and paracelsian with layered structure represented by two structural modifications: α and β , distinguished by the degree of order, are called 'hexacelsian' (Yoshiki and Matsumoto, 1951; Smith, 1953; Takeuchi, 1958; Takeuchi and Donnay, 1959; Müller, 1977; Kremenović *et al.*, 1997, 2003; Tabira *et al.*, 2000).

Gurimite is named after the geographical region of Gurim, i.e. the Gurim dome or anticline in the Hatrurim Complex in the Negev Desert, where the mineral was first found. The type specimen (authors' no. IS44b) is deposited in the mineralogical collection of the Museum of Natural History in Bern, Bernastrasse 5, CH-3005 Bern, Switzerland, catalogue number NMBE 42103. This specimen is also the holotype for zadovite, IMA2013-031.

Hexacelsian is a historical name used for >50 years to describe the synthetic phase with structure and composition analogous to the mineral described in this paper (Takeuchi, 1958). Hexacelsian is the third mineral, after celsian and paracelsian, named in honour of Anders Celsius (1701–1744), Swedish astronomer, physicist and naturalist. The type material (authors' no. IS67) is

deposited in the mineralogical collection of Mineralogical Museum, University of Wrocław (Muzeum Mineralogiczne Uniwersytetu Wrocławskiego; address: Cybulskiego 30, 50-205 Wrocław, Poland) catalogued under the number MMUWr II-20465.

Occurrence

Gurimite and hexacelsian are found in paralava of the Gurim Anticline, Negev Desert. Analysis using Raman spectroscopy (see below) indicates that gurimite is a common accessory mineral of paralavas hosted by gehlenite hornfels, whereas hexacelsian rarely occurs in these rocks. Celsian is more widespread than hexacelsian; it occurs in different types of paralava. Gurimite and hexacelsian are associated with gehlenite, pseudowollastonite, wollastonite, flamite, larnite, schorlomite, andradite, baryte, hashemite, delafossite, cuprospinel, walstromite, fresnoite, vorlanite, barioferrite, magnesioferrite, fluorapatite, fluorellestadite, hematite, perovskite, kalsilite, cuspidine, aradite, zadovite and khesinite in isolated oval polymineralic inclusions 1–2 cm in size in rankinite (Figs 1a, b) or in angular aggregates interstitial to crystals of rankinite, gehlenite, pseudowollastonite, schorlomite and fluorapatite–fluorellestadite (Figs 1a, c; 2a). These inclusions exhibit fine-grained internal structure and commonly contain skeletal and acicular minerals, some in symplectitic intergrowths, and thus differ from the surrounding rock (Figs 1b, 2a).

Gurimite, associated with minerals of the zadovite–aradite series and walstromite, was later found in paralava of Zuk (Cliff in Hebrew) Tamrur in the Negev Desert (Fig. 2b), as well as in an outcrop near the highway linking Jerusalem with the Dead Sea and Nabi Musa.

Physical and optical properties

Gurimite and hexacelsian form elongate crystals, typically <10 µm thick and <50 µm long (Fig. 1). Gurimite and hexacelsian are colourless and transparent with a white streak and vitreous lustre. The two minerals have (0001) cleavage, respectively good in gurimite and very good in hexacelsian. Fracture is irregular. Density and optical properties could not be determined due to the small size of the crystals. Density calculated using empirical formulas gave 5.044 g cm⁻³ for gurimite and 3.305 g cm⁻³ for hexacelsian. Mean refractive

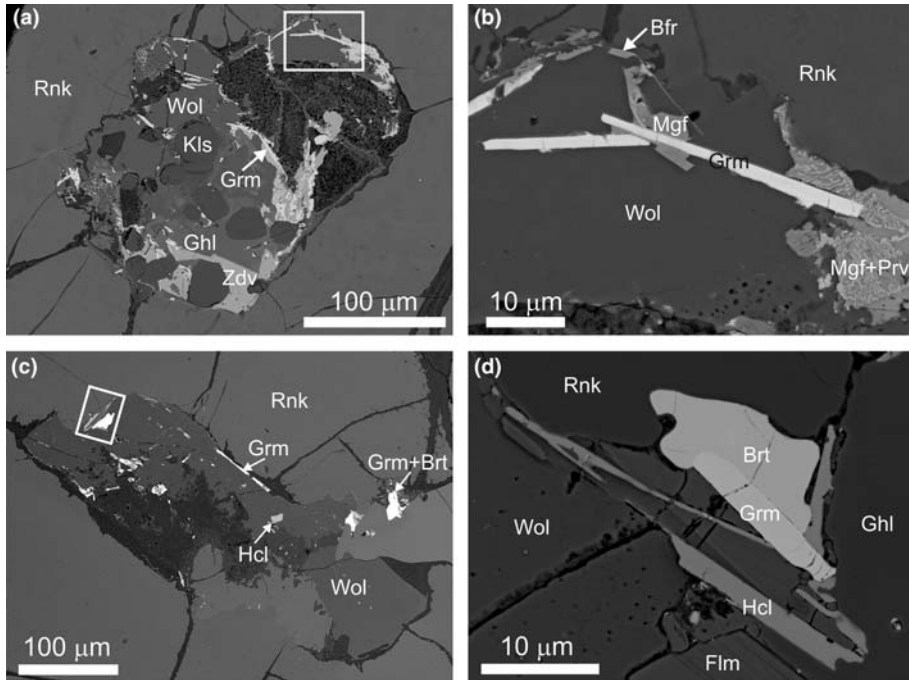


FIG. 1. Gurimite and hexacelsian in paralava of the Hatrurim Complex, Gurim Anticline, Hatrurim Basin, Negev Desert. (a) Partially replaced polymineralic inclusion in rankinite containing Ba-bearing minerals: zadovite, barioferrite, gurimite, baryte and walstromite, the frame shows an area magnified in Fig. 1b; (b) elongate [0001] crystals of gurimite; (c) polymineralic inclusions in rankinite with gurimite and hexacelsian crystals, the frame shows an area magnified in Fig. 1d; (d) elongate gurimite and hexacelsian crystals, often overgrown by baryte. Grm = gurimite, Hcl = hexacelsian, Brt = baryte, Flm = flamite, Wol = pseudowollastonite, Kls = kalsilite, Rnk = rankinite, Prv = perovskite, Mgf = magnesioferrie, Ghl = gehlenite, Zad = zadovite.

indexes, 1.945 and 1.561, respectively, were also calculated using the empirical formulas and the Gladstone-Dale relationship. Gurimite and hexacelsian are uniaxial and nonpleochroic.

Chemical composition

Composition and morphology of gurimite, hexacelsian and associated minerals was determined

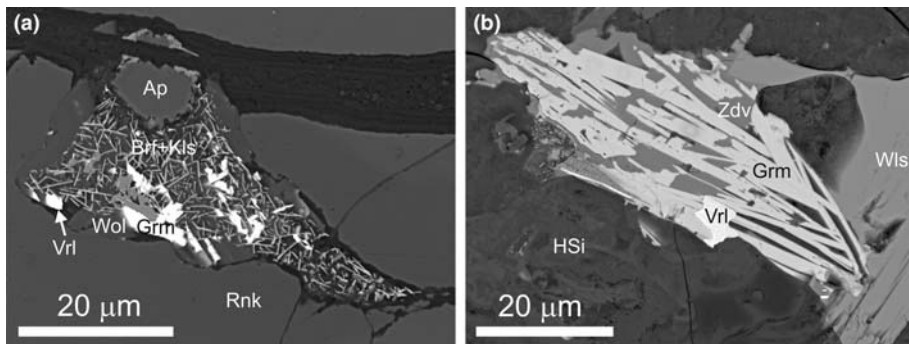


FIG. 2. (a) Fissure in rankinite infilled with partially crystallized residual high-K melt with S-bearing gurimite, paralava from East Gurim, Negev Desert; (b) high-P and Mo-bearing gurimite intergrown with zadovite in paralava from Zuk Tamur Mt, Negev Desert. Grm = gurimite, HSi = Ca-hydroxysilicate, Ap = fluorapatite, Wol = pseudowollastonite (?), Kls = kalsilite, Rnk = rankinite, Vrl = vorlanite, Wls = walstromite, Zad = zadovite, Brf = barioferrite.

using analytical scanning microscopes Philips XL30/EDAX and Phenom XL (Faculty of Earth Sciences, University of Silesia) and CAMECA SX100 and CAMECA SXFive electron microprobes (Faculty of Geology, University of Warsaw). Electron probe microanalyses were performed at 15 kV and 20 nA using the following X-ray lines and standards: BaL α , SK α – baryte; PK α – apatite; CaK α – wollastonite; SiK α – diopside; AlK α , KK α – orthoclase; TiK α – rutile; NaK α – albite, SrL α – SrTiO₃, FeK α – Fe₂O₃, CrK β – Cr₂O₃, VK α – V₂O₅, MoL α – CaMoO₄.

Holotype hexacelsian (specimen no. IS67) with empirical crystal chemical formula of (Ba_{0.911}K_{0.059}Ca_{0.042}Na_{0.010}) Σ _{1.022}Al_{1.891}Fe_{0.072}³⁺Si_{2.034}O₈ has a composition very similar to the stoichiometric BaAl₂Si₂O₈ end-member (Table 1, analysis 5). It contains negligible amounts of Fe³⁺, Ca, K and trace amounts of Na. Solid solution of hexacelsian with kokchetavite, KAlSi₃O₈, resulted in Si exceeding 2 atoms per formula unit by a small amount.

Gurimite shows marked variation in composition. Holotype gurimite from the specimen no. IS44b is close in composition to the end-member and has an empirical formula of (Ba_{2.794}K_{0.092}Ca_{0.084}Na_{0.033}Sr_{0.017}) Σ _{3.020}(V⁵⁺_{1.827}S⁶⁺_{0.091}P⁵⁺_{0.051}Al_{0.040}Si_{0.005}Fe_{0.005}) Σ _{2.017}O₈, which corresponds to: Ba₃(VO₄)₂ \approx 90%, Ba₃(PO₄)₂ \approx 5%, K₂Ba(SO₄)₂ ('Ba-palmierite') \approx 4.5% (Table 1, analysis 1).

Gurimite, associated with holotype hexacelsian (specimen no. IS67), differs in composition from the specimen no. IS44b by increased content of S and K: (Ba_{2.607}K_{0.281}Ca_{0.105}Na_{0.035}) Σ _{2.965}(V⁵⁺_{1.696}S⁶⁺_{0.213}P⁵⁺_{0.034}Cr⁶⁺_{0.025}Al_{0.048}Si_{0.016}Fe_{0.013}) Σ _{2.045}O₈, which can be calculated to give \sim 10% of a 'Ba-palmierite', K₂Ba(SO₄)₂, end-member and \sim 85% gurimite, Ba₃(VO₄)₂, end-member (Table 1, analysis 2).

The highest content of 'Ba-palmierite' end-member was established in gurimite from paralava at East Gurim (specimen no. VG6): (Ba_{2.663}K_{0.271}Ca_{0.039}Na_{0.003}) Σ _{3.003}(V⁵⁺_{1.591}S⁶⁺_{0.307}P⁵⁺_{0.058}Al_{0.035}Si_{0.006}Fe_{0.027}) Σ _{2.024}O₈, corresponding to: Ba₃(VO₄)₂ \approx 80%, K₂Ba(SO₄)₂ \approx 15%, Ba₃(PO₄)₂ \approx 5% (Table 1, analysis 3).

The occurrence of a Mo-bearing gurimite in paralava of Zuk Tamrur (specimen no. ZT19), (Ba_{2.577}K_{0.281}Ca_{0.036}Na_{0.077}) Σ _{2.971}(V⁵⁺_{1.056}S⁶⁺_{0.150}P⁵⁺_{0.653}Al_{0.048}Si_{0.020}Cr⁶⁺_{0.022}Mo_{0.087}Ti⁴⁺_{0.022}) Σ _{2.058}O₈, corresponding to Ba₃(PO₄)₂ \approx 32%, gurimite Ba₃(VO₄)₂ \approx 53%, K₂Ba(SO₄)₂ \approx 8%, K₂Ba(MoO₄)₂ \approx 5% (Fig. 2b, Table 1, analysis 4), suggests the possibility of finding a P-analogue of gurimite, Ba₃(PO₄)₂ in paralava.

Raman spectroscopy

Raman spectra (Figs 3, 4) were recorded using a WITec alpha300R Raman confocal microscope equipped with air-cooled solid-state lasers (Department of Earth Sciences, University of Silesia), emitting at 488 nm and 532 nm, and a CCD camera operating at -62°C . Raman-scattered light was focused onto a multi-mode fibre (50 μm diameter) and monochromator with a 600 mm^{-1} grating. The power of the laser at the sample position was 44 mW. Some 15–20 scans with integration time of 10–15 s and a resolution of 3 cm^{-1} were collected and averaged. The monochromators were calibrated using the Raman scattering line of a silicon plate (520.7 cm^{-1}).

The following main bands in the Raman spectrum of gurimite (cm^{-1}) were observed and assigned to (in brackets): 980 $\nu_1(\text{SO}_4)^{2-}$, 920 $\nu_1(\text{PO}_4)^{3-}$, 839 ν_1 and $\nu_3(\text{VO}_4)^{3-}$, 781 $\nu_3(\text{VO}_4)^{3-}$, 418 $\nu_4(\text{VO}_4)^{3-}$, 380 $\nu_4(\text{VO}_4)^{3-}$, 330 $\nu_2(\text{VO}_4)^{3-}$, 174 $T(\text{Ba}) + T(\text{VO}_4)^{3-}$, 136 $T(\text{Ba}) + R(\text{VO}_4)^{3-}$, 106 $T(\text{Ba})$ (Fig. 3). The Raman spectrum of gurimite with two strong bands at \sim 839 cm^{-1} and 330 cm^{-1} is identical to that of synthetic Ba₃(VO₄)₂ (Grzechnik and McMillan, 1997).

The following main bands in the Raman spectrum of hexacelsian were observed: 107, 296, 406, 461, 480, 594, 678, 809, 890, 924, 961, 1087 and 1119 cm^{-1} (Fig. 4). The Raman spectrum of hexacelsian with two strong bands at \sim 406 and 107 cm^{-1} related to $\nu_2(\text{SiO}_4)$ and ($T'M$), respectively, is similar to that of the synthetic disordered β -BaAl₂Si₂O₈ (Kremenović *et al.*, 2003). Internal modes of vibration between 100 cm^{-1} and 1100 cm^{-1} as well as some weak additional lines in a spectrum of natural hexacelsian suggests lower symmetry and/or Si⁴⁺/Al³⁺ disorder (Kremenović *et al.*, 2003).

Electron back-scattered diffraction

Gurimite and hexacelsian crystals (thickness $< 10 \mu\text{m}$) are too small for standard single-crystal X-ray diffraction, but given the availability of their synthetic analogues with known structures, the electron back-scattered diffraction method (EBSD) can be used for structural study by fitting the patterns of the minerals studied to those of synthetic analogues (Fig. 5, 6). The EBSD patterns were collected using a HKL EBSD system (HKL Technology Inc., Oxford Instruments Group) on a JEOL JSM-6480 scanning electron microscope (Institute of Materials Science, University of Silesia) using an accelerating voltage of 30 kV. Surface preparation

TABLE 1. Chemical composition of gurimite and hexacelsian from paralava of the Negev Desert, Israel.

Anal no.	Gurimite							Hexacelsian			
	Mean n = 18	1 IS44b s.d.	Range	Mean n = 13	2 IS67 s.d.	Range	3 VG6	4 ZT19	Mean n = 14	5 IS67 s.d.	Range
MoO ₃	n.d.			n.d.			n.d.	2.15	n.m.		
CrO ₃	n.d.			0.32	0.05	0.23–0.41	n.d.	0.29	n.m.		
SO ₃	1.17	0.36	0.87–1.96	2.86	0.36	2.32–3.46	4.12	2.06	n.d.		
V ₂ O ₅	26.80	0.68	25.67–27.88	25.92	0.70	24.96–27.06	24.24	16.42	n.d.		
P ₂ O ₅	0.59	0.28	0.18–1.01	0.40	0.23	0.11–0.70	0.69	7.92	n.d.		
TiO ₂	n.d.			n.d.			0.30	0.30	n.d.		
SiO ₂	0.04	0.06	0–0.25	0.16	0.07	0.09–0.32	0.06	0.21	33.06	0.25	32.62–33.48
Fe ₂ O ₃	0.04	0.04	0–0.13	0.17	0.18	0–0.59	0.36	n.d.	1.55	0.20	1.29–2.02
Al ₂ O ₃	0.33	0.02	0.29–0.36	0.41	0.03	0.36–0.46	0.30	0.42	26.07	0.23	25.66–26.39
CaO	0.76	0.28	0.44–1.59	0.99	0.54	0.30–1.80	0.37	0.35	0.64	0.31	0.30–1.20
SrO	0.33	0.08	0.23–0.45	n.d.			n.d.	n.d.	n.d.		
BaO	69.10	0.55	67.79–70.10	67.20	0.42	66.87–68.39	68.40	67.56	37.76	0.70	36.67–39.21
K ₂ O	0.70	0.15	0.53–1.01	1.72	0.21	1.40–2.08	2.14	2.26	0.75	0.03	0.70–0.81
Na ₂ O	0.16	0.02	0.13–0.19	0.18	0.02	0.15–0.23	0.16	0.41	0.08	0.01	0.07–0.11
Total	100.03			100.34			100.79	100.35	99.91		
Calculated on 8 O atoms per formula unit											
Ba	2.794			2.607			2.663	2.577	0.911		
Ca	0.084			0.105			0.039	0.036	0.042		
Sr	0.017										
K	0.092			0.218			0.271	0.281	0.059		
Na	0.033			0.035			0.030	0.077	0.010		
V ⁵⁺	1.827			1.696			1.591	1.056			
P ⁵⁺	0.051			0.034			0.058	0.653			
S ⁶⁺	0.091			0.213			0.307	0.150			
Mo ⁶⁺								0.087			
Cr ⁶⁺				0.025				0.022			
Al	0.040			0.048			0.035	0.048	1.891		
Fe ³⁺	0.003			0.013			0.027		0.072		
Si	0.005			0.016			0.006	0.020	2.034		
Ti								0.022			

s.d. – standard deviation.

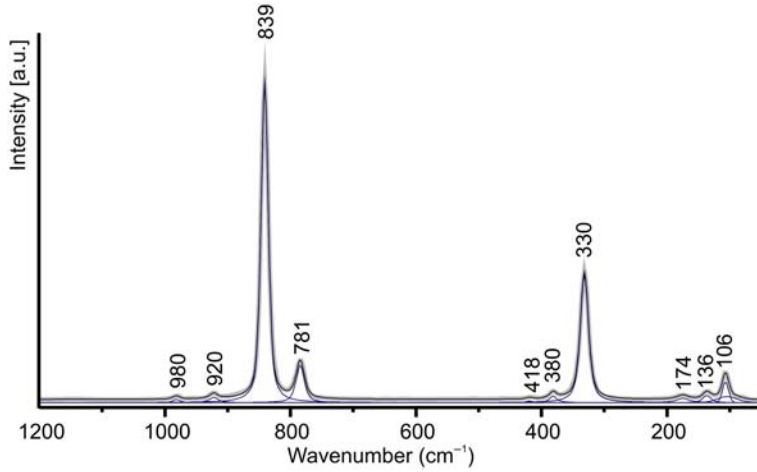


FIG. 3. Raman spectrum of gurimite, laser 488 nm.

procedure, technical parameters and the EBSD method are given in Galuskina *et al.* (2013).

The EBSD pattern for gurimite was obtained at working distances of 150 mm and 177 mm. Fitting of the EBSD pattern at 150 mm to a $\text{Ba}_3(\text{VO}_4)_2$ model (Susse and Buerger, 1970; Azdouz *et al.*,

2010) with the cell parameters $R\bar{3}m$, $a = 5.784(1)$, $c = 21.132(1)$ Å, $V = 612.2(2)$ Å³, $Z = 3$ resulted in a mean angular deviation (MAD) = 0.43° (good fit).

The EBSD pattern for hexacelsian was obtained at working distances of 155 mm and 173 mm (173 mm is an atypical working distance, which

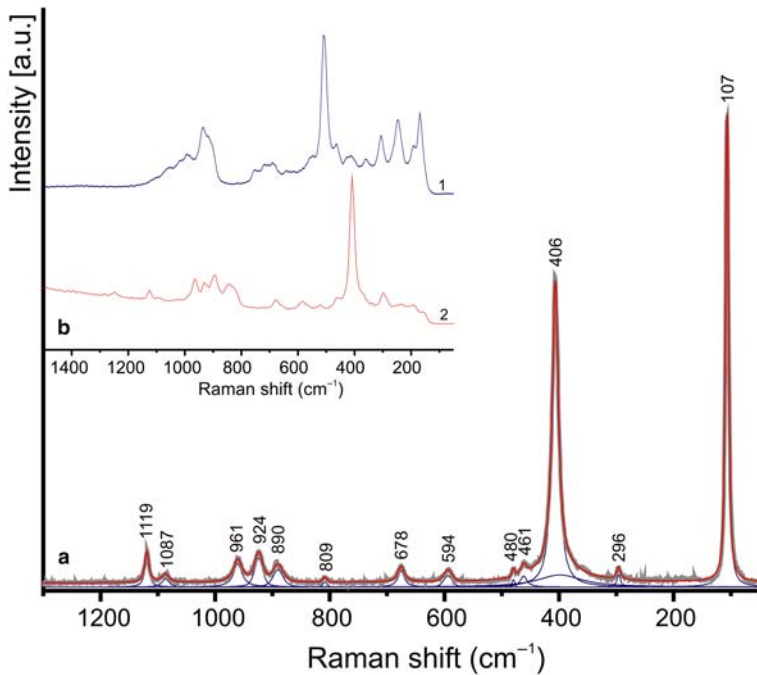


FIG. 4. (a) Raman spectrum of hexacelsian, laser 488 nm; (b) comparison of celsian (1) and hexacelsian (2) spectra, laser 532 nm.

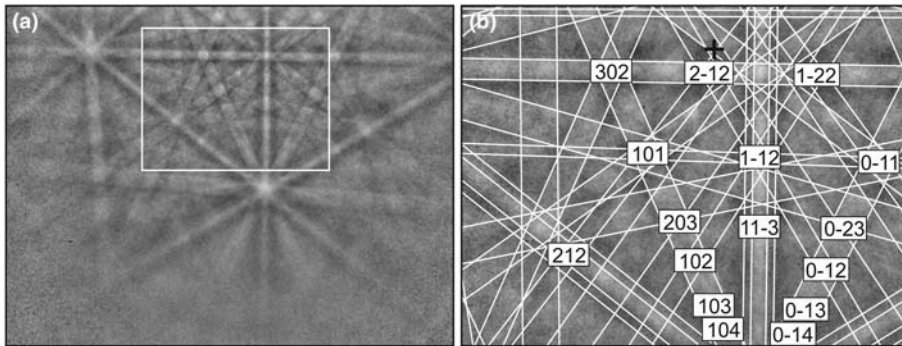


FIG. 5. (a) EBSD pattern of gurimite collected at detector distance of 177 mm and performed on a grain from Fig. 1b. The frame shows the Kikuchi pattern at detector distance of 150 mm. (b) Indexed EBSD pattern of gurimite at a detector distance of 150 mm.

was used because of apparatus technical problems). Raman data (Fig. 3) show unambiguously, that we are dealing with a phase of hexacelsian type, nevertheless models of celsian, paracelsian and

synthetic α - and β -hexacelsian were tested (Yoshiki and Matsumoto, 1951; Smith, 1953; Takeuchi, 1958; Takeuchi and Donnay, 1959; Müller, 1977; Kremenović *et al.*, 1997, 2003; Tabira *et al.*, 2000).

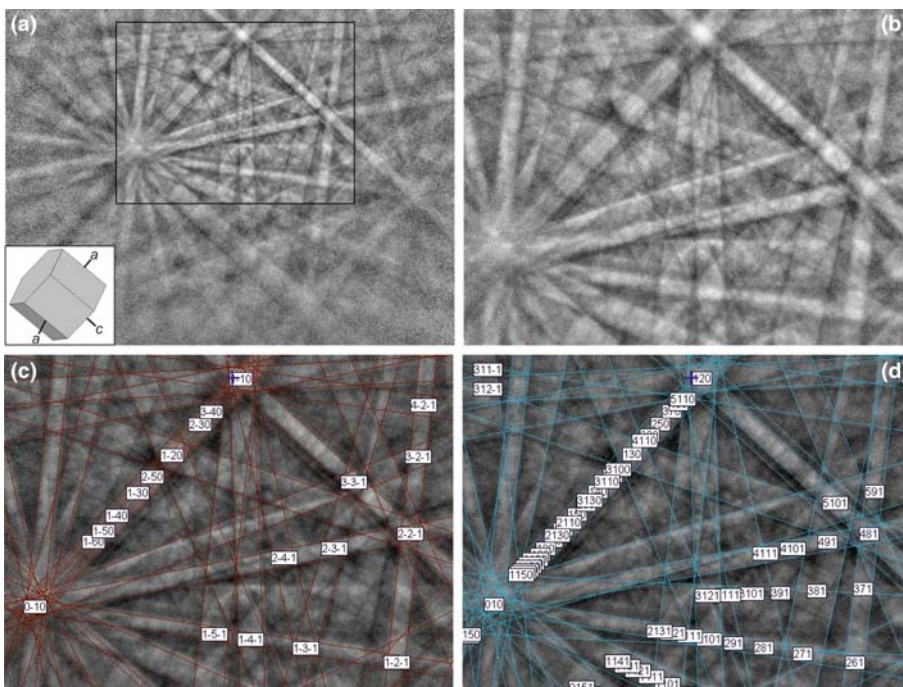


FIG. 6. (a) EBSD image obtained from a crystal shown in Fig. 1c (working distance = 173 mm, the crystal orientation is shown in the inset; the frame shows an area corresponding to the EBSD image obtained at 155 mm working distance). The EBSD data of this crystal were tested for structural model fitting to α -(pseudo)hexacelsian and β -hexacelsian; (b) EBSD image collected at work distance of 155 mm; (c, d) – fitting results for α -hexacelsian ($P6/mmm$, $c = 5.29 \text{ \AA}$, $c = 7.79 \text{ \AA}$, $\alpha = \beta = 90^\circ$, $\gamma = 120^\circ$; Takeuchi 1958) and β -hexacelsian ($P6/mmm$, $a = 5.2920(4) \text{ \AA}$, $c = 15.557(2) \text{ \AA}$, $\alpha = \beta = 90^\circ$, $\gamma = 120^\circ$; Kremenović *et al.*, 2003), respectively.

The models of 'hexacelsian' gave the best MAD = 0.51–0.59° (good fit), fitting the other models gave MAD > 3°. Although both the model of hexacelsian with parameters $a = 5.29 \text{ \AA}$ $c = 7.79 \text{ \AA}$ (Takeuchi, 1958) and the model with $a = 5.2920(4) \text{ \AA}$, $c = 15.557(2) \text{ \AA}$ (Kremenović *et al.*, 2003) give acceptable MAD, the character of Raman spectra of hexacelsian (Fig. 4) and broadening of bands in the EBSD image (Fig. 5) suggest that natural hexacelsian exhibits greater similarities to the disordered synthetic β -hexacelsian $P63/mcm$, $a = 5.2920(4) \text{ \AA}$, $c = 15.557(2) \text{ \AA}$, $\alpha = \beta = 90^\circ$, $\gamma = 120^\circ$ (Kremenović *et al.*, 2003).

TABLE 2. Calculated powder diffraction pattern for gurimite.*

h	k	L	$d_{\text{calc.}} \text{ \AA}$	I_{rel}
0	0	3	7.0962	7
1	0	1	4.8736	9
1	0	4	3.6467	6
0	1	5	3.2434	100
1	1	0	2.8906	79
0	2	1	2.4862	3
2	0	2	2.4368	14
0	0	9	2.3654	12
0	1	8	2.3498	2
0	2	4	2.2652	19
1	1	6	2.2410	7
2	0	5	2.1580	48
1	0	10	1.9591	25
0	2	7	1.9328	3
2	1	1	1.8849	2
1	1	9	1.8306	8
2	1	4	1.7830	2
1	2	5	1.7292	26
3	0	0	1.6689	13
0	2	10	1.6217	8
0	1	14	1.4550	3
2	2	0	1.4453	15
0	0	15	1.4192	1
2	1	10	1.4143	16
0	3	9	1.3636	1
3	0	9	1.3636	1
3	1	5	1.3201	10
2	0	14	1.2996	1
1	1	15	1.2740	11

* $\text{CuK}\alpha_1 = 1.540598$, Bragg-Brentano geometry, fixed slit, no anomalous dispersion; condition: $I > 1$; data were calculated using *PowderCell 2.4* (Kraus and Nolze, 1996). The strongest lines are given in bold.

Because hexacelsian and gurimite only occur in small concentrations, powder X-ray diffraction (PXRD) data could not be collected. The more reliable PXRD patterns were calculated based on the results of single-crystal structure refinements of the synthetic analogues (Tables 2, 3; Susse and Buerger, 1970; Azdouz *et al.*, 2010; Kremenović *et al.*, 2003).

Discussion

Gurimite composition, Raman spectrum and structural data obtained using EBSD revealed that gurimite is an analogue of the well-known synthetic phase $\text{Ba}_3(\text{VO}_4)_2$ (Susse and Buerger, 1970;

TABLE 3. Calculated powder diffraction data for hexacelsian.*

h	k	l	$d_{\text{calc.}} \text{ \AA}$	I
0	0	2	7.779	28
1	0	2	3.949	100
1	0	4	2.965	75
1	1	0	2.646	44
0	0	6	2.593	2
1	1	2	2.505	5
2	0	0	2.292	12
1	0	6	2.257	16
2	0	2	2.198	30
1	1	4	2.188	8
2	0	4	1.974	5
0	0	8	1.945	7
1	1	6	1.852	20
1	0	8	1.790	2
2	1	2	1.691	17
2	1	4	1.582	22
1	1	8	1.567	12
3	0	0	1.528	8
2	0	8	1.483	4
1	0	10	1.473	7
2	1	6	1.440	7
2	2	0	1.323	9
3	0	6	1.316	6
2	0	10	1.287	11
3	1	2	1.254	6
1	0	12	1.247	2
3	1	4	1.208	9
3	0	8	1.201	5

* $\text{CuK}\alpha_1 = 1.540598 \text{ \AA}$, Debye-Scherrer geometry, $I > 2$; data were calculated using *PowderCell 2.4* (Kraus and Nolze, 1996). The strongest lines are given in bold.

Grzechnik and McMillan, 1997; Zhuravlev *et al.*, 2008; Azdouz *et al.*, 2010). The gurimite structure (Fig. 7) belongs to the structural type of palmierite $K_2Pb(SO_4)_2$ ($R\bar{3}m$, $a = 5.4950(6)$, $c = 20.849(4)$ Å, $Z = 3$; Longo and Clavenna, 1976; Tissot *et al.*, 2001). Impurities of sulfur and phosphorus were incorporated into gurimite according to the isomorphous substitution scheme of $Ba^{2+} + V^{5+} \rightarrow (K, Na)^+ + S^{6+}$ and $V^{5+} \rightarrow P^{5+}$, respectively (Table 1). Barium orthovanadate $Ba_3(VO_4)_2$ has been synthesized by reactions involving solid phases at 1100–1200°C (Zhuravlev *et al.*, 2008).

Considering the high-temperature formation of paralava, chemical composition (impurities and nonstoichiometry) and the data obtained by Raman spectroscopy and EBSD, we suggest that the $BaAl_2Si_2O_8$ phase in paralava is the natural analogue of the disordered polytype – β -hexacelsian with $P63/mcm$ symmetry (analogue of synthetic β -hexacelsian) with unit-cell parameters $a = 5.292(1)$ Å, $c = 15.557(2)$ Å (Kremenović *et al.*, 2003), a suggestion consistent with the absence of the band near 183 cm^{-1} characteristic for ordered α -hexacelsian (Fig. 3, Kremenović *et al.*, 2003). Hexacelsian has a structure of the $CaAl_2Si_2O_8$ type and is a sorosilicate with a layer structure, in which Ba cations are located between ditetrahedral layers having disordered Si and Al distribution (Fig. 8).

The transition from α - to β -hexacelsian occurs at c. 300°C, and is explained by order-disorder processes (Kremenović *et al.*, 1997). At temperatures $<300^\circ\text{C}$ the disordered β -hexacelsian is metastable, but its structure can be stabilized by impurities.

We suggest that after relatively fast crystallization of the main constituents of the paralava, gurimite, hexacelsian, and also other Ba-bearing phases such as: aradite, zadovite, barioferrite, walstromite and fresnoite (Galuskin *et al.*, 2015) crystallized from small pockets of residual melt enriched in incompatible elements. Rapid crystallization of the main constituents of the paralava veins resulted in their having compositions similar to those in corresponding phases in the enclosing hornfels (Sokol *et al.*, 2008). Minerals occurring at the vein walls served as nuclei for large crystals of schorlomite–andradite, gehlenite, rankinite, pseudowollastonite and kalsilite. These crystals are usually elongated and aligned sub-perpendicularly to the vein walls. The interstices between these crystals became filled with residual melt enriched in incompatible chemical elements such as Ba, V, S, P, Ti, U, and others that were not incorporated in the early crystallized Ca-silicates and kalsilite. Study of melt inclusions in this paralava and the presence of pseudowollastonite indicate that the paralava

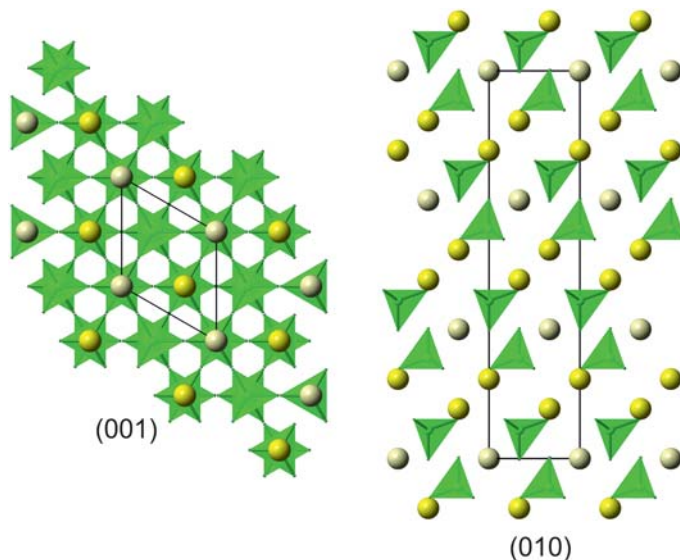


FIG. 7. Gurimite structure, it is related to palmierite ($K_2Pb(SO_4)_2$, $R\bar{3}m$) structural type, where cation layer $\{2Ba\}^{4+}$ (yellow balls – Ba_2) is located between tetrahedral $\{Ba(VO_4)_2\}^{4+}$ layers (green – V tetrahedra, light-yellow balls – Ba_1).

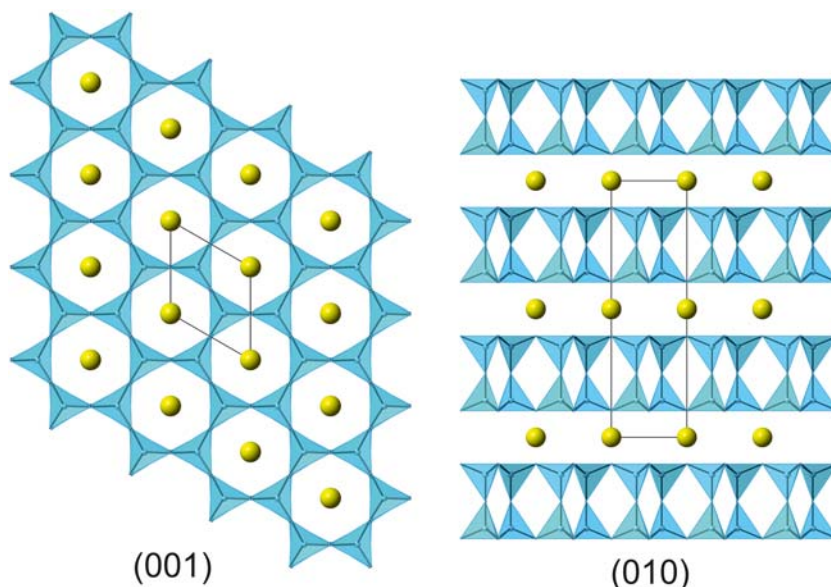


FIG. 8. Hexacelsian structure, analogous to the $\text{CaAl}_2\text{Si}_2\text{O}_8$ type. It belongs to disilicates with a layered structure where Ba cations are located between ditetrahedral layers with disordered Si and Al distribution.

minerals crystallized at temperatures $>1100^\circ\text{C}$ (Sharygin *et al.*, 2006a,b; Sokol *et al.*, 2008; Seryotkin *et al.*, 2012).

Acknowledgements

The authors thank Edward Grew (University of Maine) for English correction and useful and constructive comments. The work was supported by the National Science Centre (NCN) of Poland, grant no. UMO-2013/11/B/ST10/00272. The authors thank two reviewers (anonymous reviewer#1 and V. Sharygin) for their careful review that improved the early version of the manuscript

References

- Azdouz, M., Manoun, B., Essehli, R., Azrou, M., Bih, L., Benmokhtar, S., Ad't Hou, A. and Lazor, P. (2010) Crystal chemistry, Rietveld refinements and Raman spectroscopy studies of the new solid solution series: $\text{Ba}_{3-x}\text{Sr}_x(\text{VO}_4)_2$ ($0 \leq x \leq 3$). *Journal of Alloys and Compounds*, **498**, 42–51.
- Bentor, Y.K. (editor) (1960) Israel. In: *Lexique Stratigraphique International, Asie*, Vol. III, (10.2). Centre national de la recherche scientifique, Paris.
- Black, M.E. (2014) *Fleischer's Glossary of Mineral Species, 2014*. The Mineralogical Record Incorporated, Tucson, USA, 434 pp.
- Galuskin, E.V., Gfeller, F., Galuskina, I.O., Pakhomova, A., Armbruster, T., Vapnik, Y., Wlodyka, R., Dzierzanowski, P. and Murashko, M. (2015) New minerals with a modular structure derived from hatrurite from the pyrometamorphic Hatrurim Complex. Part II. Zadovite, $\text{BaCa}_6[(\text{SiO}_4)(\text{PO}_4)](\text{PO}_4)_2\text{F}$ and aradite, $\text{BaCa}_6[(\text{SiO}_4)(\text{VO}_4)](\text{VO}_4)_2\text{F}$, from paralavas of the Hatrurim Basin, Negev Desert, Israel. *Mineralogical Magazine*, **79**, 1073–1087.
- Galuskina, I.O., Galuskin, E.V., Prusik, K., Gazeev, V.M., Pertsev, N.N. and Dzierzanowski, P. (2013) Irinarassite $\text{Ca}_3\text{Sn}_2\text{SiAl}_2\text{O}_{12}$ – new garnet from the Upper Chegem Caldera, Northern Caucasus, Kabardino-Balkaria, Russia. *Mineralogical Magazine*, **77**(6), 2857–2866.
- Galuskina, I.O., Galuskin, E.V., Pakhomova, A.S., Widmer, R., Armbruster, T., Krüger, B., Grew, E.S., Vapnik, Ye., Dzierzanowski, P. and Murashko, M. (2017) Khesinite, $\text{Ca}_4(\text{Mg}_2\text{Fe}_{10}^{3+})\text{O}_4(\text{Fe}_{10}^{3+}\text{Si}_2)\text{O}_{36}$, a new rhönite group (sapphirine supergroup) mineral from the Negev Desert, Israel – natural analogue of SFCA phase. *European Journal of Mineralogy*, **29**(1), 101–116.
- Gross, S. (1977) The mineralogy of the Hatrurim Formation, Israel. *Geological Survey of Israel Bulletin*, **70**, 1–80.
- Grzechnik, A. and McMillan, P.F. (1997) In situ high pressure Raman spectra of $\text{Ba}_3(\text{VO}_4)_2$. *Solid State Communications*, **8**, 569–574.
- Kraus, W. and Nolze, G. (1996) POWDER CELL – a program for the representation and manipulation of

- crystal structures and calculation of resulting X-ray powder patterns. *Journal of Applied Crystallography*, **29**, 301–303.
- Kremenović, A., Norby, P., Dimitrijević, R. and Dondur, V. (1997) Time-temperature resolved synchrotron XRPD study hexacelsian $\alpha \leftrightarrow \beta$ polymorph inversion. *Solid State Ionics*, **101–103**, 611–618.
- Kremenović, A., Colomban, Ph., Piriou, B., Massiot and Florian, P. (2003) Structural and spectroscopic characterization of the quenched hexacelsian. *Journal of Physics and Chemistry of Solids*, **64**, 2253–2268.
- Longo, J.M. and Clavenna, L.R. (1976) Structural inorganic chemistry of the palmierite series $Ba_{3-x}Pb_xV_2O_8$ and its applications to catalysis. *Chemistry of Solid State Inorganics*, **272**, 45–60.
- Müller, W.F. (1977) Phase transitions and associated domains in hexacelsian ($BaAl_2Si_2O_8$). *Physics and Chemistry of Minerals*, **1**, 71–82.
- Seryotkin, Yu. V., Sokol, E.V. and Kokh, S.N. (2012) Natural pseudowollastonite: crystal structure, associated minerals, and geological context. *Lithos*, **134–135**, 75–90.
- Sharygin, V.V., Vapnik, Y., Sokol, E.V., Kamenetsky, V.S. and Shagam, R. (2006a) Melt inclusions in minerals of schorlomite-rich veins of the Hatrurim Basin, Israel: composition and homogenization temperatures. *ACROFII, Program with Abstracts*, 189–192.
- Sharygin, V.V., Vapnik, Y., Sokol, E.V. and Shagam, R. (2006b) Kalsilite-schorlomite-melilite rocks of Hatrurim Formation – products of pyrogenic alkaline melt crystallization: data on mineralogy and melt inclusions. *Abstracts of the All Russian Seminar “Geochemistry of Magmatic Rocks”*. <http://geo.web.ru/conf/alkaline/2006/index22.html> [in Russian].
- Smith, J.V. (1953) The crystal structure of paracelsian, $BaAl_2Si_2O_8$. *Acta Crystallographica*, **6**, 613–620.
- Sokol, E.V., Novikov, I.S., Zateeva, S.N., Sharygin, V.V. and Vapnik, Ye. (2008) Pyrometamorphic rocks of the spurrite-merwinite facies as indicators of hydrocarbon discharge zones (the Hatrurim Formation, Israel). *Doklady Earth Sciences*, **420**, 608–614.
- Susse, P. and Buerger, M.J. (1970) The structure of $Ba_3(VO_4)_2$. *Zeitschrift für Kristallographie*, **131**, 161–174.
- Tabira, Y., Withers, R.L., Takéuchi, Y. and Marumo, F. (2000) Structured diffuse scattering, displacive flexibility and polymorphism in Ba-hexacelsian. *Physics and Chemistry of Minerals*, **27**, 194–202.
- Takeuchi, Y. (1958) A detailed investigation of the structure of hexagonal $BaAl_2Si_2O_8$ with reference to its a–b inversion. *Mineralogical Journal*, **2**, 311–332.
- Takeuchi, Y. and Donnay, G. (1959) The crystal structure of hexagonal $CaAl_2Si_2O_8$. *Acta Crystallographica*, **12**, 465–470.
- Tissot, R.G., Rodriguez, M.A., Sipola, D.L. and Voigt, J. A. (2001) X-ray powder diffraction study of synthetic palmierite, $K_2Pb(SO_4)_2$. *Powder Diffraction*, **16**, 92–97.
- Vapnik, Y., Sharygin, V.V., Sokol, E.V. and Shagam, R. (2007) Paralavas in a combustion metamorphic complex: Hatrurim Basin, Israel. *Reviews in Engineering Geology*, **18**, 1–21.
- Yoshiki, B. and Matsumoto, K. (1951) High-temperature modification of barium-feldspar. *Journal of the American Ceramic Society*, **34**, 283–286.
- Zhuravlev, V.D., Velikodnyi, Y.A., Vinogradova-Zhabrova, A.S., Tyutyunnik, A.P. and Zubkov, V.G. (2008) $Ba_3(VO_4)_2$ – $K_2Ba(MoO_4)_2$ and $Pb_3(VO_4)_2$ – $K_2Pb(MoO_4)_2$ systems. *Russian Journal of Inorganic Chemistry*, **10**, 1632–1634.